The Astronomical Journal, 168:143 (14pp), 2024 October https://doi.org/10.3847/1538-3881/ad5956
© 2024. The Author(s). Published by the American Astronomical Society.
OPEN ACCESS

Haro 5-2: A New Pre-main-sequence Quadruple Stellar System

Bo Reipurth[1,2], C. Briceño[3], T. R. Geballe[4], C. Baranec[1], S. Mikkola[5], A. M. Cody[6], M. S. Connelley[1,12], C. Flores[7], B. A. Skiff[8], J. D. Armstrong[9], N. M. Law[10], and R. Riddle[11]
[1] Institute for Astronomy, University of Hawaii at Manoa, 640 N. Aohoku Place, HI 96720, USA; reipurth@hawaii.edu
[2] Planetary Science Institute, 1700 E Fort Lowell Rd, Suite 106, Tucson, AZ 85719, USA
[3] NSF's NOIRLab/Cerro Tololo Inter-American Observatory, Casilla 603, La Serena, Chile
[4] Gemini Observatory, 670 North Aohoku Place, Hilo, HI 96720, USA
[5] Department of Physics and Astronomy, University of Turku, Yliopistonmki (Vesilinnantie 5), Finland
[6] SETI Institute, 339 N Bernardo Ave, Suite 200, Mountain View, CA 94043, USA
[7] Institute of Astronomy and Astrophysics, Academia Sinica, 11F of AS/NTU Astronomy-Mathematics Building, No.1, Sec. 4, Roosevelt Rd, Taipei 10617, Taiwan, R.O.C.
[8] Lowell Observatory, 1400 West Mars Hill Road, Flagstaff, AZ 86001, USA
[9] Institute for Astronomy, University of Hawaii at Manoa, 34 Ohia Ku St., Pukalani, HI 96768, USA
[10] Department of Physics and Astronomy, University of North Carolina at Chapel Hill, Chapel Hill, NC 27599-3255, USA
[11] Cahill Center for Astrophysics, California Institute of Technology, 1216 East California Boulevard, Pasadena, CA 91125, USA
Received 2023 October 31; revised 2024 May 8; accepted 2024 May 10; published 2024 September 4

Abstract

We have discovered that the Hα emission-line star Haro 5-2, located in the 3–6 Myr old Ori OB1b association, is a young quadruple system. The system has a 2+2 configuration, with an outer separation of 2.″6 and with resolved subarcsecond inner binary components. The brightest component, Aa, dominates the A-binary; it is a weak-line T Tauri star with spectral type M2.5±1. The two stars of the B component are equally bright at *J*, but the Bb star is much redder. Optical spectroscopy of the combined B pair indicates a rich emission-line spectrum with a M3±1 spectral type. The spectrum is highly variable and switches back and forth between a classical and a weak-line T Tauri star. In the near-IR, the spectrum shows Paschen β and Brackett γ in emission, indicative of active accretion. A significant mid-IR excess reveals the presence of circumstellar or circumbinary material in the system. Most multiple systems are likely formed during the protostellar phase, involving flybys of neighboring stars followed by an inspiraling phase driven by accretion from circumbinary material and leading to compact subsystems. However, Haro 5-2 stands out among young 2+2 quadruples, as the two inner binaries are unusually wide relative to the separation of the A and B pair, allowing future studies of the individual components. Assuming the components are coeval, the system could potentially allow stringent tests of pre-main-sequence evolutionary models.

Unified Astronomy Thesaurus concepts: Pre-main sequence stars (1290); Binary stars (154); Multiple stars (1081); T Tauri stars (1681); Young stellar objects (1834)

Materials only available in the online version of record: data behind figures, machine-readable table

1. Introduction

The majority of stars are born as part of binary or multiple systems (for reviews, see Duchêne & Kraus 2013; Reipurth et al. 2014; Offner et al. 2023). It has even been suggested that *all* stars are born in binaries or multiples, and that the distribution of singles, binaries, and triples, etc. observed in the field is the result of subsequent dynamical interactions (Larson 1972). This is consistent with simulations (Delgado-Donate et al. 2004) and observations, which show an excess of binaries among T Tauri stars (TTSs) compared to the field (e.g., Reipurth & Zinnecker 1993) and an even higher multiplicity fraction among embedded protostars (Connelley et al. 2008; Chen et al. 2013).

While triple stellar systems have been studied extensively, both observationally as well as numerically, quadruple systems have received much less attention.

It is well established that a nonhierarchical quadruple system is unstable, and will quickly transform into a hierarchical either 2+1+1 or 2+2 configuration or break up by ejecting a single or binary star.

Many quadruple systems are known, most of them found in recent years through major sky surveys (e.g., Kostov et al. 2022, 2024). Most famous of all is ϵ Lyrae, a system of four similar A-type stars, which was first noticed by William Herschel.[13]

Detailed observational studies of quadruple systems have until recently been limited, reflecting the rarity of such systems. With the advent of deep all-sky surveys, the number of quadruple systems is rapidly increasing (e.g., Zasche et al. 2019; Fezenko et al. 2022). Although such surveys have inherent biases, they still offer new insights into the properties

[12] Staff Astronomer at the Infrared Telescope Facility, which is operated by the University of Hawaii under contract NNH14CK55B with the National Aeronautics and Space Administration.

[13] Herschel writes about ϵ Lyrae on 1778 August 29: "A very curious double–double star. At first sight it appears double at some considerable distance, and by attending a little we see that each of the stars is a very delicate double star"—Pratt & Gledhill (1880).

Original content from this work may be used under the terms of the Creative Commons Attribution 4.0 licence. Any further distribution of this work must maintain attribution to the author(s) and the title of the work, journal citation and DOI.

of quadruple systems, in particular the double eclipsing systems (Vaessen & van Roestel 2024).

A statistical study of multiplicity in F–G stars was performed by Tokovinin (2014), who finds the following percentages for singles, binaries, triples, and quadruples: 54%, 33%, 8%, and 4%. Among these quadruples, the number of 2+2 systems is higher than the 2+1+1 systems. Raghavan et al. (2010) and Riddle et al. (2015) also found a preponderance of 2+2 systems.

An understanding of this difference must be found in the early stages of evolution of quadruple systems shortly after they are formed, and hence the study of newborn quadruple systems is important. Only a few 2+2 quadruple pre-main-sequence (PMS) systems are known, among others HD 98800 (e.g., Prato et al. 2001; Zúniga-Fernández et al. 2021), FV Tau and J4872 (Correia et al. 2006), LkCa 3 (Torres et al. 2013), 2M0441+2301 (Todorov et al. 2010; Bowler & Hillenbrand 2015), EPIC 203868608 (Wang et al. 2018), and especially GG Tau (e.g., White et al. 1999; Dutrey et al. 2016), with which Haro 5-2 has a remarkable similarity in terms of configuration. Most recently, TIC 278956474 was found with the Transiting Exoplanet Survey Satellite (TESS) mission to consist of two low-mass short-period eclipsing binaries, with an age of 10–50 Myr (Rowden et al. 2020).

We here present the discovery of a new 2+2 PMS system known as Haro 5-2, located at 5:35:07.5, −2:49:00 (2000) in the Ori OB1b association (Haro & Moreno 1953). We provide detailed optical/IR imaging and spectroscopy, and discuss the properties and possible formation scenarios of this system.

2. Observations

One of us (B.A.S.) identified Haro 5-2 as a binary and it was included as SKF2259 in The Washington Visual Double Star Catalog (Mason et al. 2022). It was subsequently observed on UT 2014 November 9 using the Robo-AO autonomous laser adaptive optics system at the Palomar 1.5 m telescope (Baranec et al. 2014). We performed the observations using a long-pass filter with a cut-on wavelength of 600 nm and with a total exposure time of 3 minutes. The Ba–Bb pair is well resolved. The Aa component has an approximate image width of 0.″15, with a nonresolved elongation in the direction of Ab. The elongation was not present in the images of any other stars in the field, so we suspected this was due to an unresolved companion. To investigate this possibility, we observed Haro 5-2 with the NIRC2 instrument behind the Keck II adaptive optics system on UT 2015 August 5. We obtained six 30 s exposures with the *Kp* filter and then five 30 s exposures with the *H* filter. All four components of the Haro 5-2 system are well resolved in the *Kp* images, while the seeing degraded rapidly during the *H*-band observations, making it difficult to resolve the Aa–Ab pair. More detailed observations are required to search for additional components, as found in the similar GG Tau system (Di Folco et al. 2014).

Direct images of Haro 5-2 were obtained on UT 2015 August 27 at the Gemini-North telescope with NIRI (Hodapp et al. 2003) at $f/32$ (0.″02 pixels) and adaptive optics; see Figure 1. In the *J* and *H* bands, a 3 × 3 mosaic was obtained with individual 3 s exposures, in total 81 s, while in the *K* band the exposures totaled 162 s.

Haro 5-2 was observed with GNIRS (Elias et al. 2006) at the Gemini-North telescope on UT 2015 September 15 in a seeing of 0.″5, using 0.″05 pixels and the 10 l mm^{-1} grating in cross-dispersed mode. A 0.″15 wide slit with a length of 5.″1 was placed along the Aa–Ab pair at position angle 47°. 12 exposures each of 60 s were acquired while nodding ±1.″5 along the slit. The pair was not resolved. The slit was then changed to a position angle of 54.°3 and placed along the Ba–Bb pair. 12 exposures each of 120 s were acquired. The two components could be resolved at *H* and *K*, but not at *J*, and separate spectra were extracted in *H* and *K*. The unresolved Aa–Ab pair was reduced with the Gemini pipeline, while the Ba–Bb pair was reduced by using IRAF (Tody 1986, 1993) and Figaro (Currie et al. 2014).

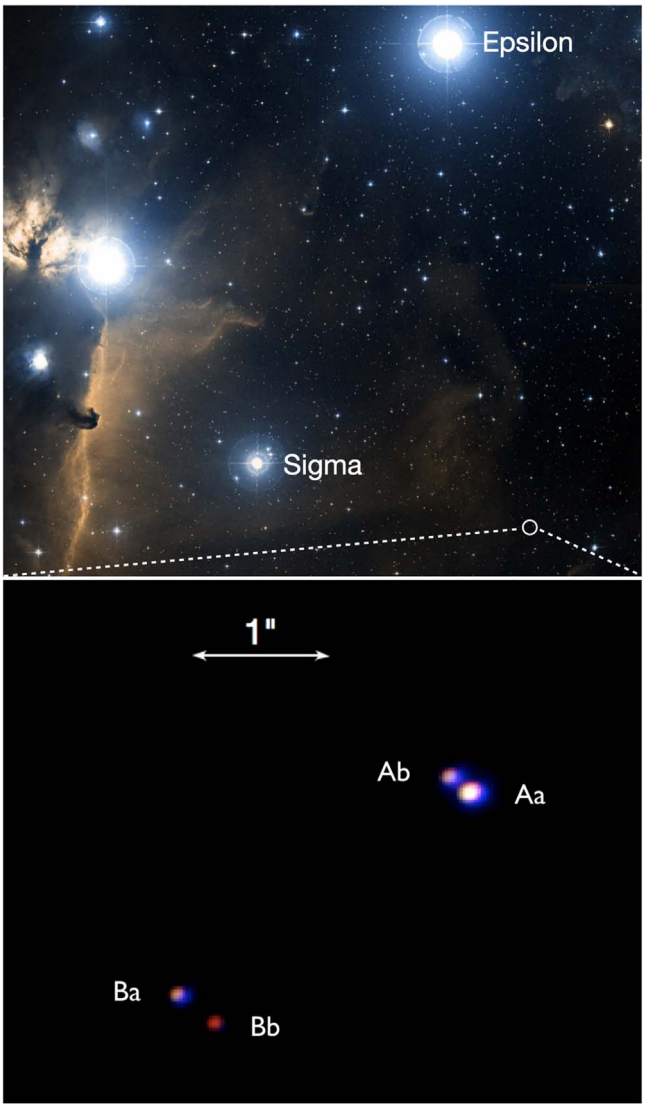

Figure 1. Top: Haro 5-2 is located in a little studied part of Orion, west of σ Ori and south of ϵ Ori, both of which are associated with groups of low-mass young stars. Image from ESASky. Bottom: near-IR *JHK* color composite of Haro 5-2 obtained with adaptive optics on the Gemini-North telescope. The small blue halos are due to a slight elongation of the *J* image.

We obtained spectroscopy of the Haro A and B components, separated by 2.″62, with the Goodman High Throughput Spectrograph (GHTS; Clemens et al. 2004), installed on the SOAR 4.1 m telescope on Cerro Pachón, Chile. We used available time slots during the engineering nights of 2021 October 19 and November 18, 2022 November 9, and 2023 January 6 and March 9, for a total time span of about 1.4 yr. GHTS is a highly configurable imaging spectrograph that

Table 1
SOAR Goodman GHTS Observations of Haro 5-2

Component	UT Date (yyyy-mm-dd)	Setup	Slit (arcsec)	Binning	Exposures ($N \times s$)
A	2021-10-20	400M1	1.0	2 × 2	3 × 120
A	2021-10-20	400M2	1.0	2 × 2	3 × 120
B	2021-10-20	400M1	1.0	2 × 2	3 × 120
B	2021-10-20	400M2	Brice1.0	2 × 2	3 × 120
B	2021-10-20	400M1	1.0	2 × 2	3 × 300
B	2021-10-20	400M2	1.0	2 × 2	3 × 300
A	2021-10-21	2100_650	0.45	1 × 2	3 × 900
B	2021-10-21	2100_650	0.45	1 × 2	3 × 1200
A	2021-11-19	400M1	1.0	2 × 2	3 × 120
A	2021-11-19	400M2	1.0	2 × 2	3 × 120
B	2021-11-19	400M1	1.0	2 × 2	3 × 300
B	2021-11-19	400M2	1.0	2 × 2	3 × 300
A	2021-11-19	2100_650	0.45	1 × 2	3 × 900
B	2021-11-19	2100_650	0.45	1 × 2	3 × 1200
A	2022-11-10	400M1	1.0	2 × 2	3 × 120
B	2022-11-10	400M1	1.0	2 × 2	1 × 300
A	2022-11-10	400M2	1.0	2 × 2	1 × 120
B	2022-11-10	400M2	1.0	2 × 2	1 × 300
A	2023-01-07	400M1	1.0	2 × 2	1 × 200
B	2023-01-07	400M1	1.0	2 × 2	1 × 400
A	2023-01-07	400M2	1.0	2 × 2	1 × 200
B	2023-01-07	400M2	1.0	2 × 2	2 × 400
A	2023-03-10	400M1	1.0	2 × 2	3 × 200
B	2023-03-10	400M1	1.0	2 × 2	2 × 600

employs all-transmissive optics and volume phase holographic gratings, resulting in high throughput for low- to moderate-resolution spectroscopy over the 320–850 nm wavelength range. We used the Goodman RED camera, which uses a deep-depletion CCD that provides extended sensitivity into the red end of the spectrum with minimal fringing. The spatial scale of the Goodman detector is $0\farcs15$ pixel^{-1}, and the slit was set at a position angle of $214\fdg7$, with the Atmospheric Dispersion Corrector active.

We configured the spectrograph for both low- and high-resolution setups. For the low-resolution setup, we used the 400 l mm^{-1} grating in its 400M1 and 400M2+GG 455 filter preset modes, with 2 × 2 binning. These two configurations combined span the wavelength range $\sim 3600 \lesssim \lambda \lesssim 9000$ Å. We used the $1''$ wide long slit, which yields an FWHM resolution = 6.7 Å (equivalent to $R = 830$). We used exposure times of 120 s for the brighter Haro 5-2A and 300 s for the fainter Haro 5-2B. A total of 21 low-resolution spectra were obtained for Haro 5-2A (13 in the 400M1 setup and eight with the 400M2 setup), while 25 spectra were obtained for Haro 5-2B (13 with the 400M1 setup and 12 with the 400M2 one), during a time window of nearly 506 days or about 1.4 yr, from UT 2021-10-20 to UT 2023-03-10 (Table 1).

For the higher-resolution spectra, we used the 2100 l mm^{-1} grating centered at 650 nm, with the $0\farcs45$ long slit, and 1 × 2 binning. This setup produces an FWHM resolution of 0.45 Å (or $R = 11{,}930$), spanning 565 Å, from 6140 Å to 6705 Å. Our choice of ×2 binning in the spatial direction improved the signal-to-noise ratio (S/N), while still matching the median $0\farcs7$ seeing at SOAR. We obtained 3 × 900 s exposures for the A component and 3 × 1200 s exposures for the B component. We took a total of six higher-resolution spectra for each of the A and B components, three each on 2021 October 21 and three each on 2021 November 19 (Table 1). The basic CCD reduction, up to and including the extraction of the 1D spectra, was carried out using the Goodman Spectroscopic Pipeline (Torres-Robledo et al. 2020). The wavelength calibration and final combination of the spectra were done with IRAF. We did not perform flux calibration, since the main purpose of our follow-up spectroscopy was to characterize each component: determining its spectral type, measuring line equivalent widths, and determining its accretion status. We measured equivalent widths of spectral features using the *splot* routine in IRAF. The S/N of the individual spectra was typically ∼20–25 at Hα, sufficient for measuring equivalent widths down to ∼0.05 Å, at our highest spectral resolution of ∼0.45 Å FWHM. In Figures 4 and 5, we show the combined spectra of Haro 5-2 obtained with the low-resolution and the higher-resolution setups, respectively. We measured equivalent widths in each of the individual spectra. The uncertainty values quoted in Tables 2 and 3 are the actual dispersion in measurement values.

On the same nights that we obtained optical spectra on SOAR, we also obtained near-IR spectroscopy resolving the Haro 5-2A and B components using the TripleSpec 4.1 (TSpec) near-IR spectrograph (Schlawin et al. 2014). The fixed-format slit is $1\farcs1$ wide and $28''$ long. The spectral resolution is $R \sim 3500$ across the six science orders. We obtained three ABBA sequences for each A and B component, using exposure times of 30 s for both components, with Fowler Sampling 4. The telluric standard HIP 26812 was observed contiguous with Haro 5-2; a single ABBA sequence was obtained at the same airmass, with an exposure time of 5 s, two coadds, and Fowler Sampling 1. The slit position angle was set at $214\fdg7$. The data were reduced in the standard way using the customized version of the IDL Spextool package (Cushing et al. 2004) that was modified by Dr. Katelyn Allers for use with TSpec at SOAR.

Haro 5-2 was observed by TESS in its sector 6 (2018 December 11 to 2019 January 7) and sector 32 (2020

Table 2
Equivalent Widths in SOAR Low-resolution Spectra of Haro 5-2

Component	Spectral Type	Type	UT DATE (yyyy-mm-dd)	W(Hα) (Å)	W(Hβ) (Å)	W(Li I) (Å)	W(Na I) (Å)	W(Ca II 8498) (Å)	W(Ca II 8542) (Å)	W(Ca II 8662) (Å)
A	M2.5	W	2021-10-20	-4.3 ± 0.1	-2.7 ± 0.1	0.4 ± 0.1	1.8 ± 0.1	0.2 ± 0.1	1.2 ± 0.1	0.9 ± 0.1
A	M2.5	W	2021-11-19	-4.1 ± 0.2	-2.6 ± 0.1	0.4 ± 0.1	1.7 ± 0.1	0.2 ± 0.1	1.3 ± 0.1	1.0 ± 0.1
A	M2.5	W	2022-11-10	-3.7 ± 0.1	-3.0 ± 0.1	0.2 ± 0.1	1.2 ± 0.1	0.3 ± 0.1	0.5 ± 0.1	0.6 ± 0.1
A	M2.5	W	2023-01-07	-4.2 ± 0.2	-3.1 ± 0.1	0.3 ± 0.1	1.8 ± 0.1	0.6 ± 0.1	1.1 ± 0.1	0.9 ± 0.1
A	M2.5	W	2023-03-10	-3.3 ± 0.1	-1.8 ± 0.1	0.2 ± 0.1	⋯	⋯	⋯	⋯
B	M3	C	2021-10-20	-20.3 ± 0.3	-5.8 ± 1.3	0.4 ± 0.1	1.8 ± 0.1	0.1 ± 0.1	0.3 ± 0.2	0.4 ± 0.1
B	M3	C	2021-11-19	-37.5 ± 0.8	-12.0 ± 0.5	0.3 ± 0.1	1.7 ± 0.1	-2.34 ± 0.1	-1.6 ± 0.1	-1.3 ± 0.1
B	M3	C	2022-11-10	-11.7 ± 0.1	-4.3 ± 0.1	0.3 ± 0.1	1.2 ± 0.1	-0.6 ± 0.1	-0.3 ± 0.1	-0.3 ± 0.1
B	M3	C	2023-01-07	-24.6 ± 0.7	-5.6 ± 0.1	0.3 ± 0.1	1.5 ± 0.1	-1.2 ± 0.1	-0.9 ± 0.1	-1.0 ± 0.1
B	M3	C	2023-03-10	-24.6 ± 2.0	-6.9 ± 2.0	0.2 ± 0.1	⋯	⋯	⋯	⋯

Notes.
(1): C = classical TTS; W = weak-line TTS.
(2): For the Na I doublet, we report the combined equivalent width of the 8183 Å and 8195 Å lines.
(This table is available in machine-readable form in the online article.)

Table 3
Hα Emission Line in SOAR High-resolution Spectra of Haro 5-2

Component	UT DATE (yyyy-mm-dd)	W(Hα) (Å)	$W10$(Hα) (km s^{-1})
Haro 5-2A	2021-10-21	-7.08 ± 0.13	198.6 ± 3.6
Haro 5-2A	2021-11-19	-3.69 ± 0.03	165.7 ± 2.7
Haro 5-2B	2021-10-21	-18.73 ± 0.24	420.8 ± 2.8
Haro 5-2B	2021-11-19	-37.73 ± 0.62	552.2 ± 2.9

November 19 to 2020 December 17) campaigns, which lasted approximately 27 days each. Known as TIC 427380741 in the TESS Input Catalog, Haro 5-2 was monitored in full-frame image ("FFI") mode. Sector 6 images were acquired at a cadence of 30 minutes, while those for sector 32 were taken every 10 minutes. The TESS mission data products for FFI targets do not include light curves, and so we downloaded stacked 15×15 pixel cutout images in the form of target pixel files (TPFs) using the `lightkurve` package (Lightkurve Collaboration et al. 2018). In these images, Haro 5-2 appears clearly in the center, approximately two pixels offset from the nearest relatively bright source. To create a lightcurve, we placed a 3×3 pixel square aperture on the source, summing the flux at each available time. `lightkurve` was used to carry out this procedure, as well as to subtract out a star-free average background. TESS light curves of different targets often exhibit common systematic trends due to scattered light, which can be removed by detrending against flux time series of pixels outside the target aperture. We employed the `lightkurve` RegressionCorrector class to remove low-level trends in the Haro 5-2 light curves, using the top two principal component vectors. We ultimately removed points for which the original image TPF data were flagged in the TESS pipeline as being contaminated by stray light. The resulting light curves displayed a series of significant undulations on a range of timescales, similar to what was seen in the raw time series.

3. Observational Results

3.1. Haro 5-2

Haro 5-2, also known as 2MASS J05350753-0248596 and ESO-Hα 1108 (Pettersson et al. 2014), is located in the Ori OB1b association. As discussed in the following, we conclude that it is a young stellar object (YSO), based on its Hα emission, its mid-IR excess, its irregular variability, and its location within a star-forming region.

In the first survey for Hα emission stars in the σ Ori region, Haro & Moreno (1953) discovered 98 objects, including Haro 5-2, which was also detected in the Hα emission-line survey by Weaver & Babcock (2004). The σ Ori cluster has an age of 3–5 Myr and contains several hundred young low-mass stars (e.g., Caballero 2008a; Hernández et al. 2014; Koenig et al. 2015).

Haro 5-2 is located in a little studied region southwest of the cluster of young stars surrounding the O9.5 V multiple star σ Ori. Schaefer et al. (2016) measured the distance to σ Ori itself as 387.5 ± 1.3 pc, while Caballero (2018) used Gaia DR2 for all known members of the σ Ori cluster to derive a mean distance of 391 ± 44 pc.

Caballero (2008b) stated that "the cluster seems to have two components: a dense core that extends from the center to $r \sim 20'$ and a rarefied halo at larger distances." This halo extends to $\sim 30'$, whereas Haro 5-2 has a separation to σ Ori of almost 1°. Consequently, Haro 5-2 may alternatively be part of the loose clustering Collinder 70 surrounding ε Ori, also known as Alnilam (Collinder 1931; Caballero & Solano 2008). The σ Ori and Collinder 70 populations together form the subgroup Ori OB1b, defined by Blaauw (1964). Kounkel et al. (2018) suggest that Ori OB1b is located at a distance of 357 ± 3 pc and has an age of 3–6 Myr. Figure 1(a) shows the location of Haro 5-2 relative to σ Ori and ε Ori.

Haro 5-2 is not an isolated Hα emission star; Haro & Moreno (1953) found three other Hα emitters, Haro 5-1, 5-3, and 5-4, within a few arcminutes, and within 10′, Pettersson et al. (2014) found another five: ESO-Hα 1011, 1014, 1050, 1146, and 1364. A variable YSO, V2070 Ori, is also located close to Haro 5-2. Using Gaia DR3 parallaxes for the stars in this little group (omitting the multiple system Haro 5-2 itself and also Haro 5-3, for neither of which Gaia has a parallax) suggests a mean distance of 373 ± 13 pc, which we adopt.

Haro 5-2 is not directly associated with any cloud, but a small cloudlet, Dobashi 4834, is located about 15′ to the southwest (Dobashi 2011) and is part of the shell of gas and dust that has been pushed away from the central O star σ Ori; see Figure 1 of Koenig et al. (2015), which shows a Wide-field Infrared Survey Explorer (WISE) three-color image mosaic of the region.

Given their youth, the components of Haro 5-2 are likely to be variable, and a g-lightcurve from ASASSN (Shappee et al. 2014; Kochanek et al. 2017) of the integrated system light indeed shows irregular variability over a 5 yr period, with characteristic amplitudes of 0.1–0.2 mag. TESS has observed the region including Haro 5-2 on two occasions (see Section 2) and the light curves are shown in Figure 2. The light curves vary with peak-to-peak amplitudes of ∼7% and are largely of a stochastic type that may indicate accretion variability (Cody et al. 2014). This irregular variability likely originates in the B components, of which at least one is a classical TTS (CTTS; see Section 3.3.2). In addition, the data from sector 32 exhibit several upward excursions of a few percent amplitude that are reminiscent of distinct accretion bursts (Cody et al. 2017).

Since we are viewing the combined light of several stars, it is possible that multiple variability types are represented in the time series. For each lightcurve, we computed a Fourier transform periodogram and searched for persistent signals. We find one tentative periodicity in common between both TESS light curves, at a timescale of 1.33 days (sector 6) to 1.36 days (sector 32) and an amplitude of ∼0.7%. These detections are tentative, since the light curves are dominated by higher-amplitude stochastic behavior; the S/N in the periodogram is 3.2 (sector 6) to 3.6 (sector 32), whereas a secure detection would require an S/N value of at least 4.0 (e.g., Breger et al. 1993). If real, the possible periodic signals could be indicative of starspots on one member of Haro 5-2, probably component Aa, which is significantly brighter than the other stars.

3.2. IR Imaging

Figure 1(b) shows a multicolor *JHK* image of Haro 5-2, obtained with adaptive optics at the Gemini-North 8 m telescope, in which Haro 5-2 is well resolved as a 2+2 quadruple system. What makes Haro 5-2 of particular interest is that the two close pairs have rather large projected separations Aa–Ab and Ba–Bb relative to the projected separation of A–B compared to other PMS quadruple systems. If not purely a

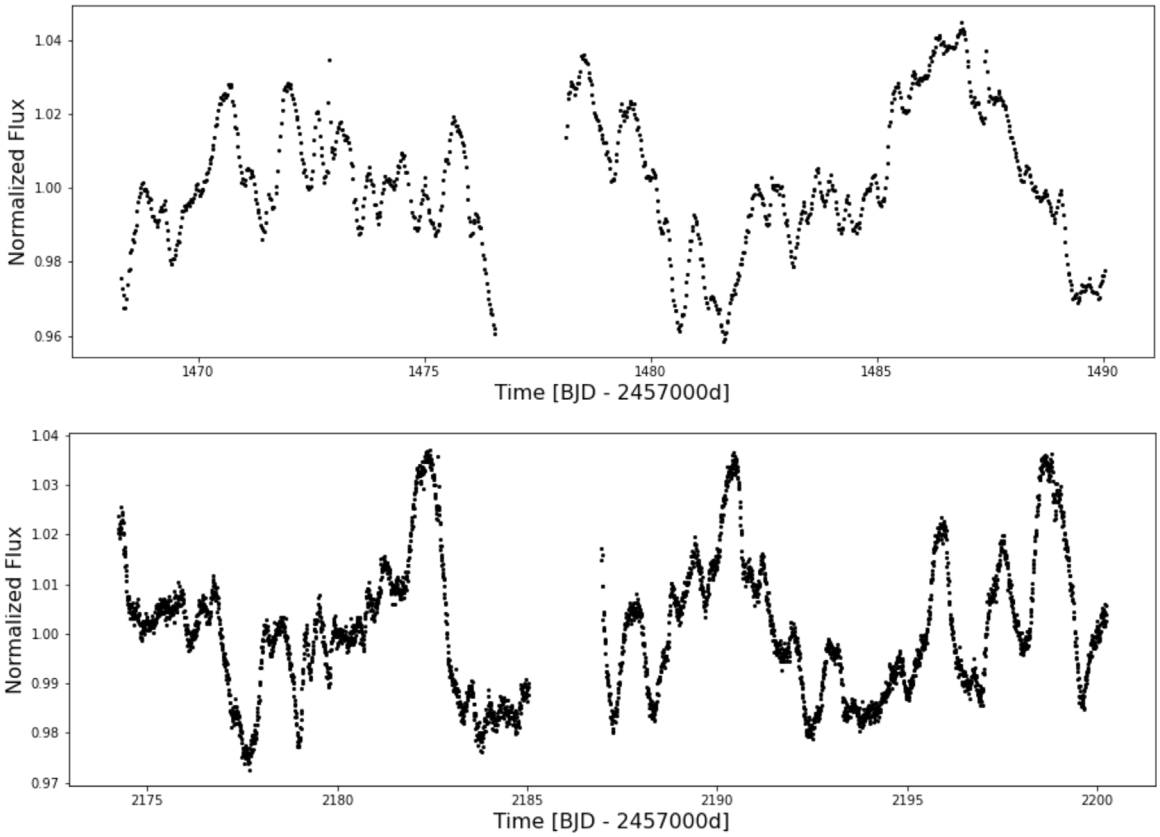

Figure 2. TESS light curves of the combined light from the four components of Haro 5-2 from around 2018 December (Sector 6; top) and around 2020 December (Sector 32; bottom). For Sector 6, the cadence was once every 30 minutes, and for Sector 32, it was once every 10 minutes.

projection effect, this might be due to its youth, with the four components still interacting before settling into a long-term stable configuration in which the inner binaries have hardened.

We have measured the separations for the three pairs and determined the following separations for Aa–Ba: 2.″61 (975 au); Aa–Ab: 0.″19 (72 au); and Ba–Bb: 0.″35 (131 au). Also, Andrei Tokovinin kindly observed the system with the high-resolution speckle camera at the SOAR telescope (Tokovinin et al. 2022) and these values are listed in Table 4. The projected separation of the A and B binaries of about 1000 au may suggest a period around 30,000 yr. The closest binary, Aa–Ab, has a period of ∼1000 yr, which will be measurable in a time span of a few years.

Photometry of the components from the Gemini data on UT 2015 August 27 yields:

Aa: $K = 11.53$ $H - K = 0.40$;
Ab: $K = 12.34$ $H - K = 0.30$;
Ba: $K = 12.46$ $H - K = 0.34$; and
Bb: $K = 12.54$ $H - K = 0.92$.

The uncertainties in H and K are around 0.02 mag. While the three brighter components have roughly the same colors, Bb is extremely red, suggesting that this component is either highly extincted, has a strong near-IR excess, or a mixture of the two.

Haro 5-2 has been detected in a number of sky surveys, from the ultraviolet (Skymapper) to the mid-IR (WISE). Figure 3 shows the available photometry together with four WISE panels that reveal the system to be bright at IR wavelengths. We have integrated over the energy distribution of the quadruple, and derive a luminosity of 0.95 $L_\odot$ between 0.35 and 22 μm. The peak of the energy distribution is around 1.05 μm, which corresponds to about 2760 K. According to the temperature–spectral type conversion by Herczeg & Hillenbrand (2014), this corresponds to an M7 spectral type. As discussed below, this classification is not borne out by spectroscopy. The energy distribution, although dominated by the brightest member, Aa, is not from a single object, but includes the three fainter components, thus shifting the peak in Figure 3 to longer wavelengths. Also, Haro 5-2 shows Hα emission, a sign that accretion is occurring and indicating the presence of circumstellar material that further adds to an IR excess. Thus, much of the light seen at longer wavelengths is not likely to come from the dominant member Aa. In fact, almost half of the observed luminosity, 0.43 $L_\odot$, falls within the four WISE bands.

Table 4
Separation and Position Angles of Haro 5-2 Pairs

Pair	PA (deg.)	Sep. (arcsec)	Proj. Sep. (au)	ΔI (mag)
Aa,Ba	124.9 ± 0.8	2.6130 ± 0.0008	975	···
Aa,Ab	54.7 ± 0.8	0.1942 ± 0.0008	72	1.0
Ba,Bb	233.0 ± 1.3	0.3504 ± 0.0013	131	0.7

Notes.
(1): Observed by Andrei Tokovinin on 2021.7983 with the HRCam speckle camera at the SOAR telescope in good seeing (Tokovinin et al. 2022).
(2): The data for the Ba–Bb pair are noisy.
(3): Projected separations for a distance of 373 pc.

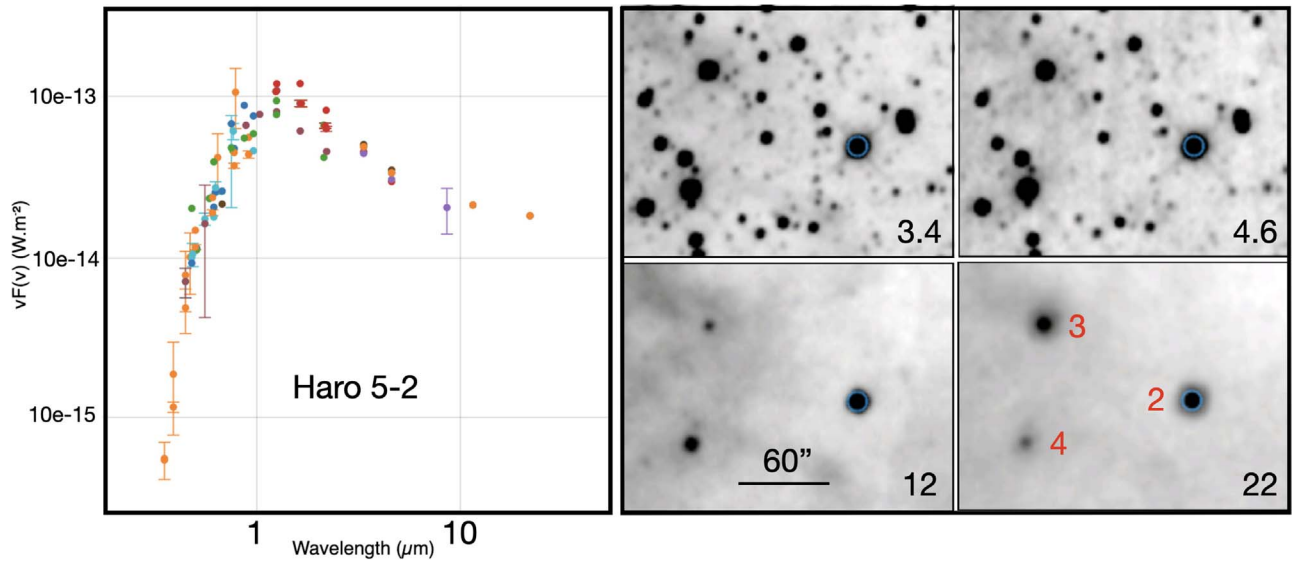

Figure 3. Left: spectral energy distribution from SIMBAD of the integrated light from the Haro 5-2 quadruple with data from SkyMapper, the Sloan Digital Sky Survey, PanSTARRS, Johnson, the Two Micron All Sky Survey, AKARI, and WISE. Right: WISE images with Haro 5-2, 5-3, and 5-4 marked. The field is about 0.84 pc wide at the distance of Haro 5-2.

3.3. Optical Spectroscopy

Haro & Moreno (1953) discovered the T Tauri nature of Haro 5-2 on the basis of its Hα emission, and it remains a prominent Hα emission-line star (Pettersson et al. 2014). Figure 4 shows optical low-resolution spectra of the (unresolved) A and B binaries, obtained with the GHTS instrument at SOAR (Section 2).

Both the A and B binaries have the TiO absorption bands characteristic of M-type dwarfs. By comparing our spectra with spectra of already known M-type TTSs from the extensive sample of Briceño et al. (2019), we assign spectral types of M2.5 for Haro 5-2A and M3 for Haro 5-2B, with an overall uncertainty of one subclass. As can also be seen in Figure 4, both the A and B binaries exhibit a clear Li I 6708 Å absorption line, with equivalent widths W(Li I)$\sim$0.3 Å. Li I is a well-known indicator of youth for late-type stars (e.g., Briceño et al. 1998, 2001; White & Basri 2003). Because lithium is depleted during the PMS stage in the deep convective interiors of K- and M-type stars, a late-type star is classified as a TTS if it has Li I (6707 Å) in absorption, with an equivalent width larger than that of a zero-age main-sequence Pleiades star of the same spectral type (Soderblom et al. 1993; García López et al. 1994). The Na I 8183,8195 Å absorption doublet is also a well-known feature useful for discriminating young, late-type PMS stars from their field dwarf counterparts (Martín et al. 1996; Lawson et al. 2009; Lodieu et al. 2011; Hillenbrand et al. 2013; Hernández et al. 2014; Suárez et al. 2017; Briceño et al. 2019). Consistent with the presence of Li I, both Haro 5-2A and B exhibit weak Na I absorption (Figure 4), with values expected for TTSs with ages of a few megayears (e.g., see Figure 13 in Briceño et al. 2019).

3.3.1. Haro 5-2A

The low- and higher-resolution spectra show that the Hα line of the brighter A binary exhibits a small equivalent width, with an average value $W(\mathrm{H}\alpha) = -3.9$ Å, and a range -3 Å $\geqslant W(\mathrm{H}\alpha) \geqslant -4$ Å, during the $\sim$1.4 yr over which we obtained multi-epoch spectroscopy (Tables 2 and 3). In addition to the low intensity of the emission, the Hα line profile is narrow, $\lesssim$200 km s^{-1}, as measured in the high-resolution spectra (Figure 5). These characteristics are indicative of Hα originating in the active chromosphere of a young dwarf. The low intensity of Hα places the A binary in the weak-line TTS (WTTS) class (see Figure 6).

3.3.2. Haro 5-2B

In contrast with its brighter sibling, Haro 5-2B shows a strong Hα emission line, which is also broad when seen in detail in the higher-resolution spectra. Moreover, thanks to our many observing epochs (Tables 2 and 3), we find that the emission is highly variable, ranging from $W(\mathrm{H}\alpha) = -38.5$ Å in 2021 November to a low $W(\mathrm{H}\alpha) = -11.6$ Å a year later, in 2022 November. We derive an average $W(\mathrm{H}\alpha) = -24.6$ Å. The width of the Hα line ranges from $\sim$400 to $>$500 km s^{-1} and exhibits a very strong, slightly blueshifted absorption, suggestive of a strong wind. Moreover, the entire Balmer series is found to be in emission (Figure 4), with $-3.6 \lesssim W(\mathrm{H}\beta) \lesssim -12.3$ Å. The Ca H and K 3934,3968 Å lines are also in emission, with equivalent widths in the range W(Ca H and K) ~ -3 to ~ -15 Å. Both He I 5876 Å and He I 6678 Å are also found in emission, with W(He I 5876) ~ -2.1Å and W(He I 6678) ~ -1.2 Å. The Ca II near-IR triplet goes from being weakly in absorption during the 2021 October observation, when Haro 5-2B was in a seemingly more quiescent state, to being in emission, and staying in this state, from 2021 November to 2023 January. Unfortunately, we could not obtain spectra with the reddest 400M2 configuration during the 2023 March observation. We determine average values of W(Ca II 8498) $= -1.7$ Å, W(Ca II 8542) $= -1.1$ Å, and W(Ca II 8662) $= -1.0$ Å.

The rich assortment of H, He, and Ca emission lines seen in Haro 5-2B, together with the strength of the Hα emission, the broad wings of several hundred kilometers per second in its line profile, and the strong, slightly blueshifted central absorption are all indicative of a strongly accreting CTTS, as can be seen by the location of this object in the diagnostic diagrams of Figures 6 and 7. The blueshifted central absorption

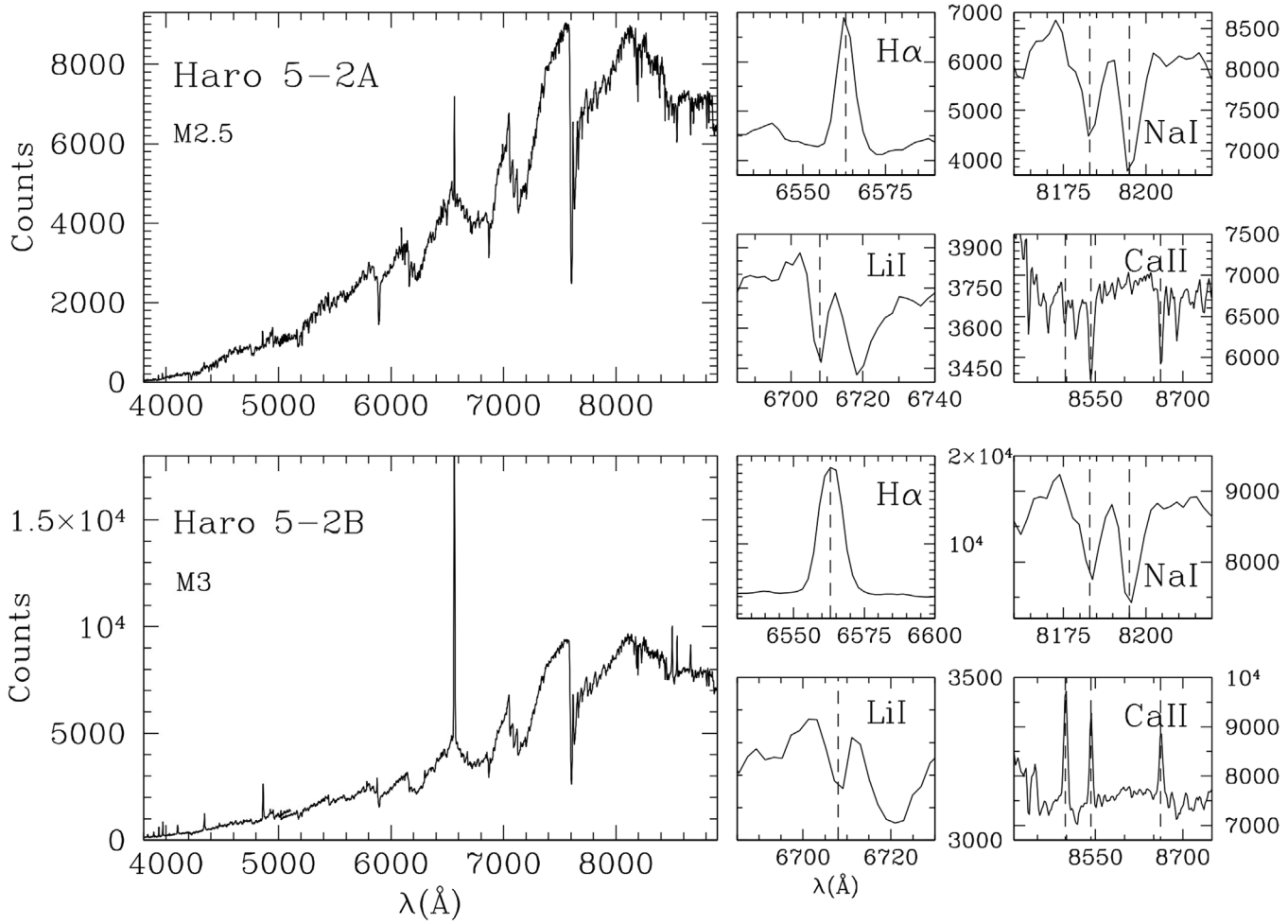

Figure 4. Low-resolution optical spectra of the Haro 5-2A and B components, as obtained on UT 2021-11-19 with the GHTS instrument at SOAR. In the upper panels, the M2.5 WTTS Haro 5-2A component has Hα weakly in emission. In the lower panels, the accreting M3 CTTS Haro 5-2B component has a strong Hα emission line and the entire Balmer series is in emission. Lithium is moderately strong. Ca H and K are also found strongly in emission, as well as the He I lines. Finally, the Ca II near-IR triplet is in emission.

(The data used to create this figure are available in the online article.)

is seen with similar strength in both the October and November observations.

We highlight the importance of obtaining multi-epoch spectra and of combining low- and higher-resolution spectra, in order to provide both the wide spectral coverage needed to derive a reliable spectral type ($T_{\rm eff}$) and the resolving power to characterize the Hα line profile, thus allowing the correct classification of young PMS stars such as Haro 5-2. If we observed this object only in November, we would have misclassified Haro 5-2B as a WTTS or C/W (Figure 6). It is the multi-epoch low-resolution spectroscopy, combined with the higher-resolution spectra, that allows us to confirm that the B component is a CTTS and that A is a WTTS. In particular, the higher-resolution spectra show that despite variations in both the strength of Hα and the velocity width, at both epochs, Haro 5-2A remains well inside the region populated by nonaccreting, young, PMS low-mass stars, whereas the B-binary is well within the region where strongly accreting young PMS stars are found.

3.3.3. Masses

The optical spectra of Haro 5A (M2.5) and 5B (M3) are dominated by the components Haro 5Aa and 5Ba, respectively. If we assume a temperature uncertainty of 0.5 subtypes, we find that $T_{\rm eff}$(Aa) $\sim 3485 \pm 80$ K and $T_{\rm eff}$(Ba) $\sim 3410 \pm 100$ K, using the spectral-type-to-temperature conversion of Herczeg & Hillenbrand (2014). For an assumed age of 3 Myr, the magnetic models of Feiden (2016) suggest that Aa has a mass of $0.54 \pm 0.08\,M_{\odot}$ and Ba has a mass of $0.46 \pm 0.1\,M_{\odot}$. However, Braun et al. (2021) and Flores et al. (2022) have shown that magnetic models overpredict masses for young stars with $M_{*} < 0.4\,M_{\odot}$. Nonmagnetic Feiden models give $M_{\rm Aa} = 0.35 \pm 0.05\,M_{\odot}$ and $M_{\rm Ba} = 0.31 \pm 0.08\,M_{\odot}$. Given the uncertainties in both spectral types and in models, we end up with the not very accurate estimate of $M_{\rm Aa} \sim 0.45 \pm 0.15\,M_{\odot}$ and $M_{\rm Ba} \sim 0.35 \pm 0.15\,M_{\odot}$. The Ab and Bb components are likely to have somewhat lower masses. A rough estimate of the system mass is therefore $\sim 1.5\,M_{\odot}$.

3.4. IR Spectroscopy

The near-IR spectra of the Haro 5-2A and 5-2B (unresolved) binaries obtained with the TSpec near-IR spectrograph at the SOAR telescope are shown in Figure 8. Both objects display metal absorption lines and CO bands and a triangular *H*-band continuum due to water absorption, all consistent with their optical late spectral types. The spectrum of Haro 5-2A (upper

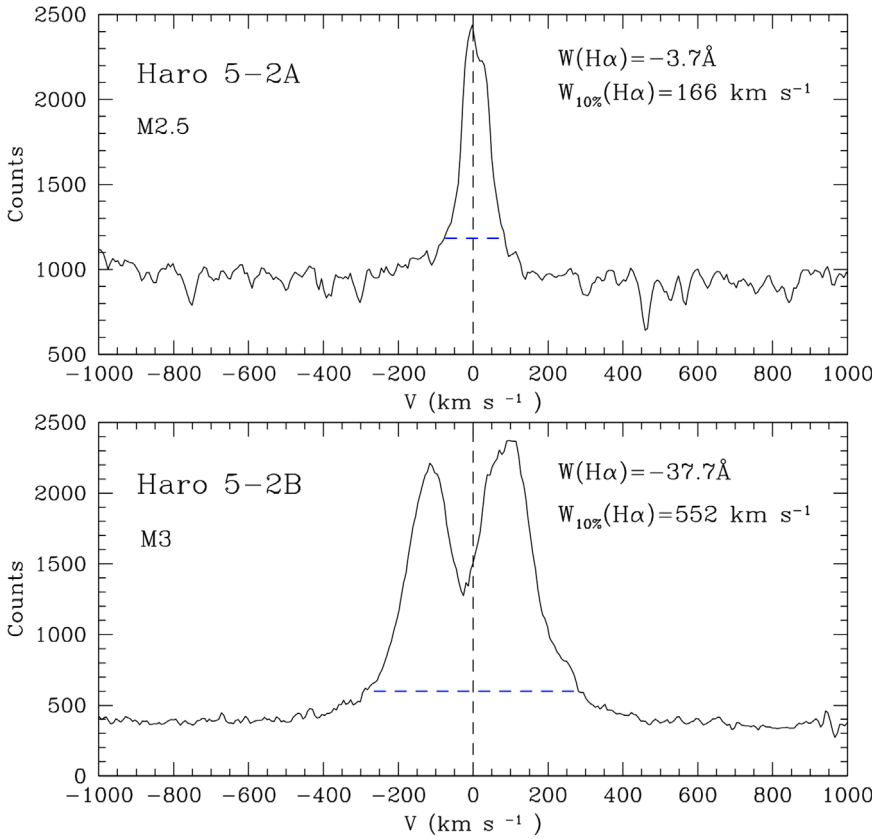

Figure 5. High-resolution spectra of the Hα line of the Haro 5-2A and B components, obtained with the SOAR GHTS on UT 2021-11-19. Upper panel: spectrum of the M2.5 WTTS Haro 5-2A. Lower panel: spectrum of the accreting M3-type CTTS Haro 5-2B. The vertical dashed line is set at the rest wavelength for Hα (6562.8 Å). The blue horizontal dashed line indicates the full width of the Hα profile at 10% of its full height (White & Basri 2003).
(The data used to create this figure are available in the online article.)

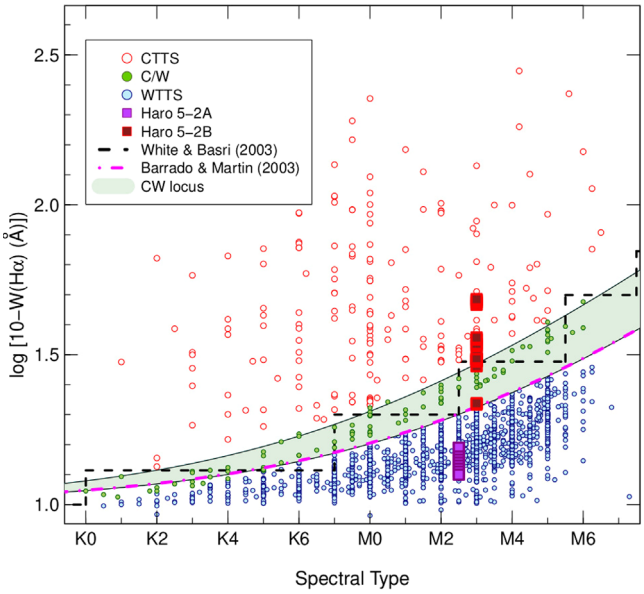

Figure 6. Equivalent width of Hα (plotted as $\log_{10}(10 - W(\mathrm{H}\alpha))$ as a function of spectral type for Haro 5-2A and B, at each epoch for which we obtained low-resolution spectra at SOAR. Haro 5-2A is plotted as large purple boxes, and Haro 5-2B as large red boxes. For comparison, the Orion TTSs from Briceño et al. (2019) are also shown: CTTSs as red circles, and WTTSs as smaller blue dots. The separation between CTTS and WTTS as defined by White & Basri (2003) is shown with the black dashed line, while the criterion adopted by Barrado et al. (2011) is plotted as a dashed–dotted magenta line. The transition region adopted by Briceño et al. (2019) between CTTS and WTTS is shown by the pale green region where C/W objects fall (shown as green dots).

panel) shows no emission features, consistent with its classification as a nonaccreting WTTS, as shown in Figures 6 and 7. In contrast, the spectrum of Haro 5-2B (lower panel) displays strong Paschen β and Brackett γ emission lines, indicative of active accretion. The near-IR spectra, obtained on the same nights as the optical spectra, are thus consistent with the optical classifications.

Line variability is always an issue when observing young stars, and we note that a near-IR spectrum of the (blended) A binary obtained with GNIRS on 2015 September 15 showed a broad Paschen β line in emission, and a very weak emission at Brackett γ, indicating that active accretion was taking place at the time. On the same night, the B-binary was also observed with GNIRS using adaptive optics, and the two components Ba and Bb were resolved. The *H*-band spectra of the two B components are shown in Figure 9. The spectra are almost identical, but the Bb component shows much more veiling as well as a redder continuum. This indicates that the deep red color of the Bb component seen in the bottom panel of Figure 1 is not due to a much later spectral type than Ba, but rather to a strong near-IR excess.

4. Discussion

4.1. Formation of Quadruple Systems

As pointed out by Larson (1972), multiple stars are a natural consequence of the collapse of a rotating cloud core, and many if not all stars may originate in such systems. Observationally, it is well established that in most star-forming regions there is

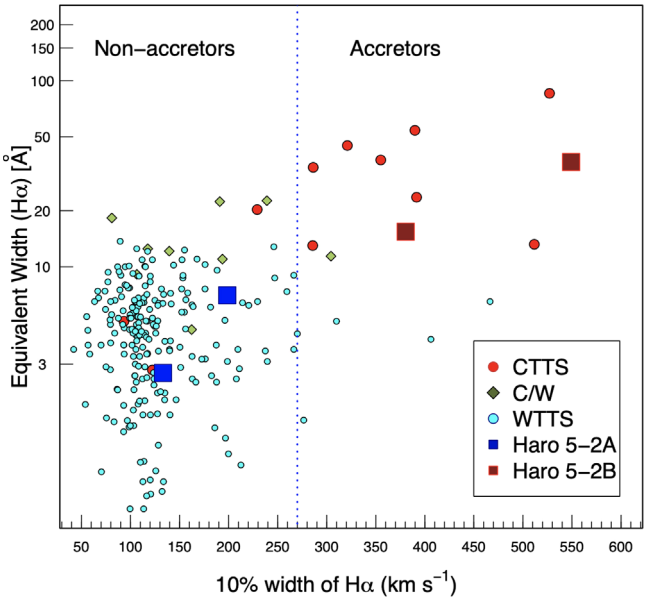

Figure 7. Equivalent width of Hα as a function of the 10% width of the Hα line profile, for Haro 5-2A (large blue boxes) and Haro 5-2B (large red boxes), measured in the two epochs during which we obtained high-resolution spectra at SOAR. Data are also shown for the Orion TTS from Briceño et al. (2019): CTTSs as red dots, WTTSs as smaller cyan dots, and C/Ws as green diamonds. The separation between CTTSs and WTTSs as defined by White & Basri (2003) is shown with the vertical blue dashed line at 270 km s^{-1}.

an excess of young binaries and multiples relative to the field population (e.g., Leinert et al. 1993; Reipurth & Zinnecker 1993). It follows that to get down to the number in the field, there must be considerable dynamical evolution during early stellar evolution, from *N*-body interactions in combination with the presence of gas in the system.

The 2+1+1 quadruples are easily formed from small nonhierarchical systems with four or more components through dynamical interactions that lead to subsequent ejections of members into distant bound orbits or into escapes (e.g., Delgado-Donate et al. 2004). The more common 2+2 systems, on the other hand, have been explained in a variety of ways.

Bodenheimer (1978) suggested that successive fragmentations of a cloud core with transfer of spin angular momentum at each stage would lead to wide binary systems in which each component is a close binary. Such a cascade would naturally lead to 2+2 quadruples with large ratios between inner and outer orbits, although hydrodynamical simulations generally show more chaotic and sequential star formation. The inner binaries of Haro 5-2 are well above the opacity limit to fragmentation, so this scenario might describe the formation of Haro 5-2.

Whitworth (2001) considered a different type of cascade, in which two colliding clouds form a shock-compressed layer that fragments into filaments and cores and eventually form stars with massive disks. Collisions of two disks around binaries can form bound quadruple systems.

While turbulent core fragmentation will produce wider binaries and multiples (100–10,000 au), simulations of this process fail to produce the very close binaries often found in 2+2 quadruples. To produce such close binaries, a dissipative gaseous environment is required, in which orbital decay will harden a binary (e.g., Bate et al. 2002; Delgado-Donate et al. 2004; Lee et al. 2019; Guszjenov et al. 2023; Kuruwita & Haugbolle 2023).

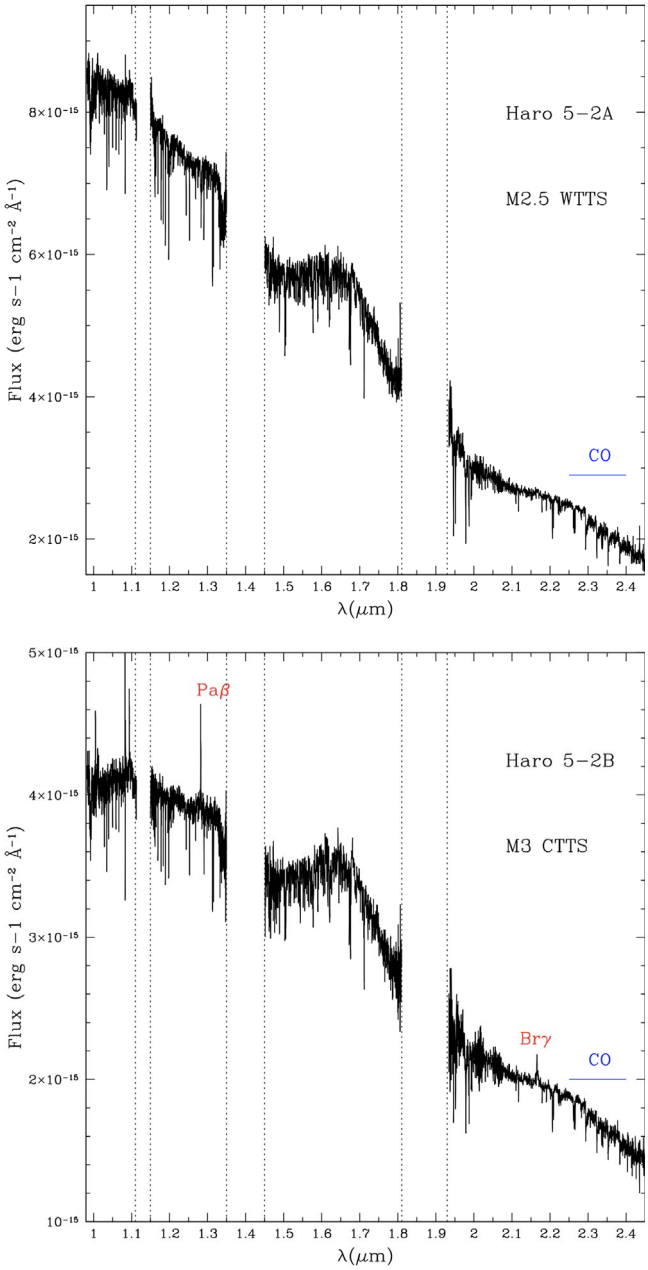

Figure 8. Near-IR spectra of Haro 5-2A and Haro 5-2B obtained with TSpec at the SOAR telescope. Note the Paβ and Brγ emission lines in Haro 5-2B. Wavelength intervals with strong terrestrial opacity are excluded.
(The data used to create this figure are available in the online article.)

In disk fragmentation models, massive disks can become gravitationally unstable and produce one or more companions and, combined with capture, 2+2 systems can be formed (Kratter & Lodato 2016). Filament fragmentation has also been discussed as leading to bound binaries and multiples (e.g., Bonnell & Bastien 1993; Pineda et al. 2015; Sadavoy & Stahler 2017).

van Albada (1968a, 1968b) carried out *N*-body simulations of small-*N* groups (10 to 24 stars), treating the stellar components as point sources and noting that among the final outcomes were a number of 2+2 quadruples. The dynamical evolution of such gas-free quadruple systems has subsequently been further studied by many other authors (e.g.,

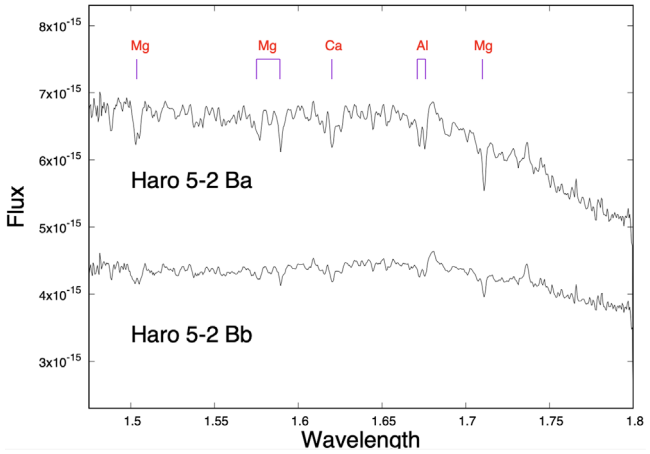

Figure 9. *H*-band spectra of the individual Ba and Bb components resolved with adaptive optics and GNIRS at the Gemini-North 8 m telescope. Wavelength is in microns and flux is in $\mathrm{Wm}^{-2}\ \mu\mathrm{m}^{-1}$.
(The data used to create this figure are available in the online article.

Harrington 1974; Mikkola 1983, 1984a, 1984b; Sterzik & Durisen 1998).

To summarize, it appears that there are multiple viable pathways to the formation of 2+2 quadruple stellar systems, and the multiple systems we observe in the field may result from a mix of different formation scenarios.

4.2. The Origin of the Haro 5-2 Quadruple System

In the following, we discuss three questions regarding the structure, stability, and formation of the Haro 5-2 system.

(1) *Is Haro 5-2 merely a chance alignment of two young binaries along the line of sight?*

We have photometric and spectroscopic evidence that the components of Haro 5-2 are young, so we look at the surface density of nearby young stars. In an area of roughly $25' \times 30'$ centered on Haro 5-2, there is a small group of only nine additional YSOs. This immediately indicates that the probability that Haro 5-2A and Haro 5-2B are close due to a chance alignment along the line of sight is negligible.

(2) *Is Haro 5-2 a temporary quadruple or can it be in a stable configuration?*

Compared to other PMS quadruples, the most remarkable aspect of Haro 5-2 is the large separations of the two inner binaries relative to the outer binary when compared to other known young 2+2 quadruple systems.[14] This opens the question of whether Haro 5-2 in the future might break apart.

For a definite answer, one would need to know the orbits of the Haro 5-2 components, or at least the physical separations in the system, the stellar masses, and the velocities of the components. None of this is currently known. Instead, we have performed some statistical estimates for a variety of system properties. For these calculations, we have assumed that Aa has a mass of about 0.45 $M_\odot$ and the three other components have masses of about 0.35 $M_\odot$, in total 1.5 $M_\odot$, which determines the gravitational potential. We have further assumed that the centers of mass of the two subsystems are in the plane of the sky, since this would be the most unstable configuration, while the orbital planes of the subsystems are random. Finally, we adopted random velocities assuming virial balance. We then ran a code, described in more detail in Reipurth & Mikkola (2015), which computes semimajor axes, eccentricities, and other orbital characteristics for bound systems. After 10,000 experiments, about one-third remained stable 2+2 quadruples. Given that Haro 5-2 almost certainly is extended along the line of sight and thus more stable, we conclude that the quadruple may well be in a long-term stable configuration.

(3) *Could Haro 5-2 have become a quadruple at a later stage after dispersal of most of the placental gas?*

If Haro 5-2 had already formed as a quadruple during the embedded collapse phase, one would expect that the resulting dynamical evolution in a gaseous environment and active accretion would lead to a decrease of the semimajor axes of the inner binaries, thus producing harder inner binaries (e.g., Bate et al. 2002). This is not what is seen in Haro 5-2, which has well-resolved inner binaries, suggesting that it might have developed its 2+2 configuration sufficiently late to have avoided early shrinking of the two inner binaries during the gas-rich embedded phase. This could have resulted in two spectroscopic binaries, as in the young 2+2 quadruples LkCa 3, EPIC 203868608, and TIC 278956474, mentioned earlier. Consequently, we have explored numerically the dynamical evolution of a small cluster of single and binary stars at a later stage, after the bulk of the gas has dispersed or been accreted, to see if *N*-body simulations without gas could result in a quadruple like Haro 5-2, following the pioneering work of van Albada (1968a, 1968b). We have performed many thousands of new numerical simulations with 4-, 10-, 20-, and 50-body groups of single stars and masses drawn from the initial mass function and with virialized velocities (see Reipurth et al. 2010; Reipurth & Mikkola 2015 for details of the code). Some binary and multiple systems indeed do form, including at least temporarily some 2+2 quadruples (see Figure 10(a)).

However, if one assumes that a substantial fraction of the bodies are binaries, then, not surprisingly, 2+2 systems are formed more frequently (see Figure 10(b)). We conclude that the number of individual members of the initial multiple system is much less important than whether some of those members are binaries.

Such 2+2 quadruples can form without the help of a gaseous environment when three objects, of which at least two are binaries, interact chaotically, in the process binding the two binaries together into a 2+2 quadruple system, leaving the third body (single or binary) to carry away the excess energy. It should be noted that the binaries survive these interactions only if they have binding energies that exceed the gravitational perturbations induced by flybys. Effectively, the binaries have to act almost as point sources; that is, they must be close relative to the impact parameter. Thus, the stable 2+2 quadruples formed this way are highly hierarchical, like ϵ Lyrae, because wider subsystems would be disrupted during the chaotic formation process. It follows that to form 2+2 quadruples this way, the two binaries must previously have undergone a process that makes them "hard." This, however, would not form the more open architecture of Haro 5-2.

Haro 5-2 is a member of the Ori OB1b association and is therefore not a case of isolated star formation. Within the previously mentioned little group of young stars surrounding Haro 5-2, the two closest are the Hα emitters Haro 5-3 and

[14] The ratio of projected outer and inner separations is 7.4. However, the boundary between chaotic and regular orbits is dependent on many parameters, not least the eccentricity (Valtonen & Karttunen 2006), and a single value cannot grasp this complexity. But at least, for comparison, the ratio is 7.3 for HIP 28442, and since the star is a member of the old thick-disk population, it has evidently been stable for a long time (Tokovinin 2020).

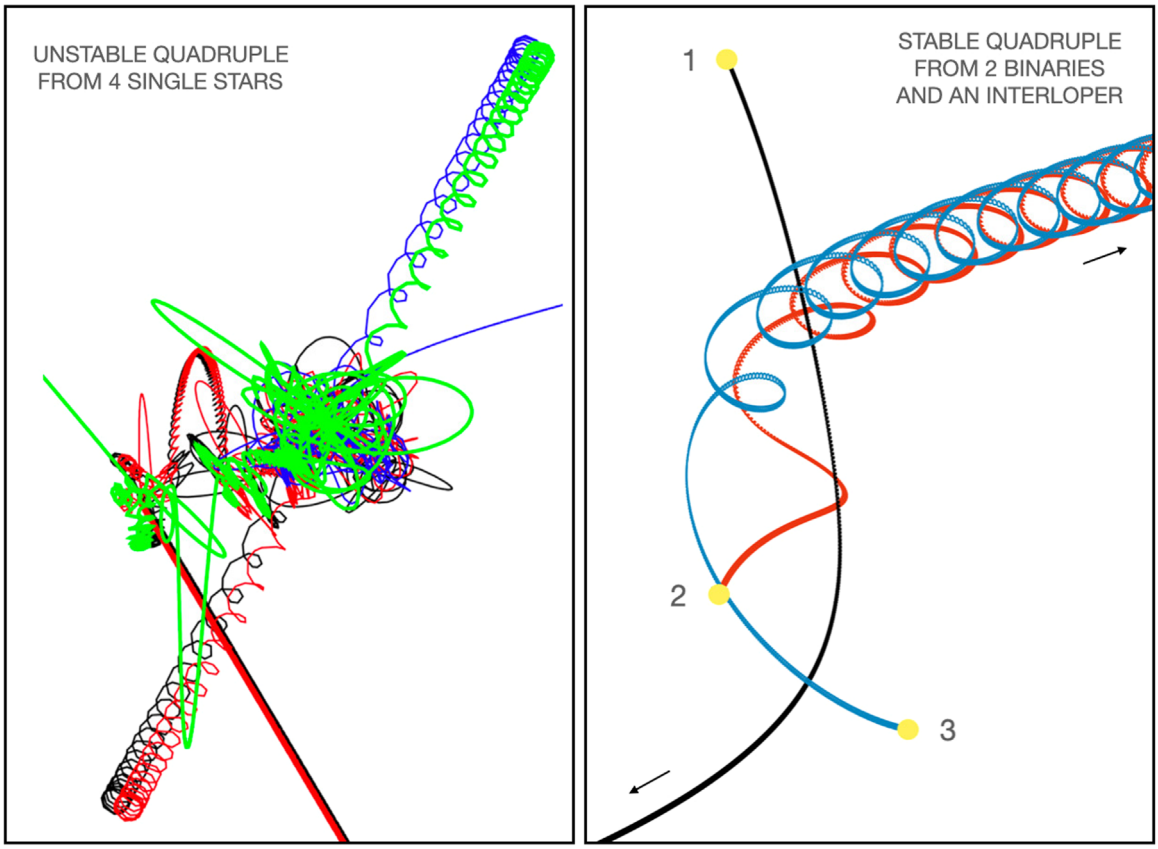

Figure 10. Left: example of chaotic transformation of a nonhierarchical system of four single stars into a temporary 2+2 quadruple (black/red + blue/green), which subsequently breaks up into a binary (black/red) and two single stars (blue and green). Right: example of a nonhierarchical configuration of two primordial binaries (2 and 3) that bind to form a stable 2+2 quadruple system, as an interloper flies by and carries away the excess energy. The formation of a quadruple system is far simpler when the binaries have formed prior to their interaction. Both simulations show the dynamical interactions of point sources without any gas.

Haro 5-4 (see Figure 3), which are both only about 3.′6 away. This corresponds to about 80,000 au or 0.4 pc in projection, which—assuming a stellar velocity dispersion of $\sim$1 km s^{-1}—can be traversed in less than half a million yr. Haro 5-4 has a faint companion to the NNW, which has an IR excess to 12 μm and possibly to 22 μm, as seen in WISE images, and thus could be a young star, too. It is therefore conceivable that the Haro 5-2 system in the past could have been part of a larger group that broke up, with Haro 5-3 and 5-4 carrying away the energy that enabled the Haro 5-2A and B binaries to bind together into a 2+2 system.

5. Conclusions

1. We have discovered a new young 2+2 quadruple system, Haro 5-2, in the 3–6 Myr old Ori OB1b association, which encompasses the σ Ori and the Collinder 70 clusterings. The system has an overall extent of 2.″6 and projected separations of the inner binaries of 0.″19 and 0.″35.
2. We obtained low-resolution optical spectra of both the A and B components of the Haro 5-2 quadruple system on five nights over $\sim$1.5 yr, as well as two high-resolution spectra separated by about a month. The presence of significant TiO absorption molecular bands in the spectra, combined with indicators of stellar youth, such as the Li I 6708 Å and Na I 8183,8195 Å absorption features, confirm these as low-mass, young PMS stars. The brighter A component is a nonaccreting M2.5-type ($T_{\rm eff} \sim 3450$ K) WTTS. The fainter B component is an M3-type ($T_{\rm eff} \sim 3400$ K) accreting CTTS, but on two nights it fell in the transition region between CTTS and WTTS. Overall, the emission in both stars varies by up to a factor 2× over the course of our observations. Assuming evolutionary models such as Feiden (2016), these spectral types correspond to a mass $\sim$0.35–0.45 $M_{\odot}$. The Hα profile of the accreting B component shows broad wings extending to $\sim \pm$300 km s^{-1}, and a strong, slightly blueshifted central absorption. This blueshifted absorption is seen in the higher-resolution spectra at both epochs. The Bb component is very red and the spectrum may be affected by accretion and by extinction from a circumstellar disk.
3. The hierarchy of Haro 5-2 is low; i.e., the two inner binaries in Haro 5-2 are unusually wide relative to the separation between the two binaries in comparison with other known PMS quadruples. We have made simulations of a variety of configurations and conclude that the system may well survive intact over long timescales.
4. Since the members of the Haro 5-2 quadruple are well resolved and presumably of the same age, this system may provide stringent constraints on PMS evolutionary models, similar to the well-studied pentuple GG Tau. Haro 5-2 also displays a significant IR excess, and Atacama Large Millimeter/submillimeter Array observations of its circumstellar material may offer insights into the effect of flybys on disks.

Acknowledgments

We thank A. Tokovinin and J. A. Caballero for valuable comments, and A. Tokovinin for providing the data in Table 4.

Based in part on observations obtained at the International Gemini Observatory, a program of NSF's NOIRLAB, which is managed by the Association of Universities for Research in Astronomy (AURA), under a cooperative agreement with the National Science Foundation, on behalf of the Gemini partnership: the National Science Foundation (United States), the National Research Council (Canada), Agencia Nacional de Investigación y Desarollo (Chile), Ministerio de Ciencia, Tecnologia e Innovación (Argentina), Ministerio da Ciencia, Technologia, Inovacoes e Comunicacoes (Brazil), and the Korea Astronomy and Space Science Institute (Republic of Korea).

It is also based in part on observations obtained at the Southern Astrophysical Research (SOAR) telescope, which is a joint project of the Ministério da Ciência, Tecnologia e Inovações (MCTI/LNA) do Brasil, the US National Science Foundation's NOIRLab, the University of North Carolina at Chapel Hill (UNC), and Michigan State University (MSU). IRAF was distributed by the National Optical Astronomy Observatory, which was managed by the Association of Universities for Research in Astronomy (AURA), under a cooperative agreement with the National Science Foundation.

The Robo-AO system is supported by collaborating partner institutions, the California Institute of Technology, the Inter-University Centre for Astronomy and Astrophysics, the National Science Foundation under grant Nos. AST-0906060, AST-0960343, and AST1207891, a grant from the Mt. Cuba Astronomical Foundation, and a gift from Samuel Oschin.

This paper includes data collected by the TESS mission. Funding for the TESS mission is provided by NASA's Science Mission Directorate.

This research has made use of the SIMBAD database, operated at CDS, Strasbourg, France, and of NASA's Astrophysics Data System Bibliographic Services.

This research made use of Astropy, a community-developed core Python package for Astronomy (Astropy Collaboration et al. 2013, 2018, 2022). We are grateful to Katelyn Allers for her detailed and instructive YouTube videos on reducing TSpec data: https://www.youtube.com/user/katelynallers/videos.

Facilities: PO: 1.5m (Robo-AO), Keck: II (NIRC2-LGS), Gemini-Gillett (GNIRS,NIRI), SOAR (Goodman spectrograph, TSpec spectrograph, HRCam).

Software: Astropy, IRAF, TOPCAT (Taylor 2005), Lightkurve (Lightkurve Collaboration et al. 2018).

ORCID iDs

Bo Reipurth https://orcid.org/0000-0001-8174-1932
C. Briceño https://orcid.org/0000-0001-7124-4094
T. R. Geballe https://orcid.org/0000-0003-2824-3875
C. Baranec https://orcid.org/0000-0002-1917-9157
S. Mikkola https://orcid.org/0000-0003-1448-8767
A. M. Cody https://orcid.org/0000-0002-3656-6706
M. S. Connelley https://orcid.org/0000-0002-8293-1428
C. Flores https://orcid.org/0000-0002-8591-472X
B. A. Skiff https://orcid.org/0000-0001-5306-6220
N. M. Law https://orcid.org/0000-0001-9380-6457
R. Riddle https://orcid.org/0000-0002-0387-370X

References

Astropy Collaboration, Price-Whelan, A. M., Lim, P. L., et al. 2022, ApJ, 935, 167
Astropy Collaboration, Price-Whelan, A. M., Sipőcz, B. M., et al. 2018, AJ, 156, 123
Astropy Collaboration, Robitaille, T. P., Tollerud, E. J., et al. 2013, A&A, 558, A33
Baranec, C., Riddle, R., Law, N. M., et al. 2014, ApJL, 790, L8
Barrado, D., Stelzer, B., Morales-Calderón, M., et al. 2011, A&A, 526, A21
Bate, M. R., Bonnell, I. A., & Bromm, V. 2002, MNRAS, 336, 705
Blaauw, A. 1964, ARA&A, 2, 213
Bodenheimer, P. 1978, ApJ, 224, 488
Bonnell, I., & Bastien, P. 1993, ApJ, 406, 614
Bowler, B., & Hillenbrand, L. 2015, ApJL, 811, L30
Braun, T. A. M., Yen, H.-W., Koch, P. M., et al. 2021, ApJ, 908, 46
Breger, M., Stich, J., Garrido, R., et al. 1993, A&A, 271, 482
Briceño, C., Calvet, N., Hernandez, J., et al. 2019, AJ, 157, 85
Briceño, C., Hartmann, L., Stauffer, J., & Martín, E. 1998, AJ, 115, 2074
Briceño, C., Vivas, A. K., Calvet, N., et al. 2001, Sci, 291, 93
Caballero, J. A. 2008a, A&A, 478, 667
Caballero, J. A. 2008b, MNRAS, 383, 375
Caballero, J. A. 2018, RNAAS, 2, 25
Caballero, J. A., & Solano, E. 2008, A&A, 485, 931
Chen, X., Arce, H. G., Zhang, Q., et al. 2013, ApJ, 768, A110
Clemens, J. C., Crain, J. A., & Anderson, R. 2004, Proc. SPIE, 5492, 331
Cody, A. M., Hillenbrand, L. A., & David, T. J. 2017, ApJ, 836, 41
Cody, A. M., Stauffer, J., Baglin, A., et al. 2014, AJ, 147, 82
Collinder, P. 1931, On Structuralproperties of Open Galactic Clusters and their Spatial Distribution (Lund: Nya Boktryckeriet)
Connelley, M. S., Reipurth, B., & Tokunaga, A. T. 2008, AJ, 135, 2526
Correia, S., Zinnecker, H., Ratzka, T., & Sterzik, M. F. 2006, A&A, 459, 909
Currie, M. J., Berry, D. S., Jenness, T., et al. 2014, in ASP Cpnf. Ser. 485 Astronomical Data Analysis and Systems, ed. N. Manset & P. Forshay (San Francisco, CA: ASP), 391
Cushing, M. C., Vacca, W. D., & Rayner, J. T. 2004, PASP, 116, 362
Delgado-Donate, E. J., Clarke, C. J., Bate, M. R., & Hodgkin, S. T. 2004, MNRAS, 351, 617
Di Folco, E., Dutrey, A., Le Bouquuin, J.-B., et al. 2014, A&A, 565, L2
Dobashi, K. 2011, PASJ, 63, S1
Duchêne, G., & Kraus, A. 2013, ARAA, 51, 269
Dutrey, A., Di Folco, E., Beck, T., & Guilloteau, S. 2016, A&ARv, 24, 5
Elias, J. H., Rodgers, B., Joyce, R., et al. 2006, Proc. SPIE, 6269, 14
Feiden, G. A. 2016, A&A, 593, A99
Fezenko, G. B., Hwang, H.-C., & Zakamska, N. L. 2022, MNRAS, 511, 3881
Flores, C., Connelley, M. S., Reipurth, B., & Duchêne, G. 2022, ApJ, 925, 21
García López, R. J., Rebolo, R., & Martin, E. L. 1994, A&A, 282, 518
Guszjenov, D., Raju, A. N., Offner, S. S. R., et al. 2023, MNRAS, 518, 4693
Haro, G., & Moreno, A. 1953, Bol. Obs. Tonantz. Tacub., 1, 11
Harrington, R. S. 1974, CeMec, 9, 465
Herczeg, G. J., & Hillenbrand, L. 2014, ApJ, 786, 97
Hernández, J., Calvet, N., Pérez, A., et al. 2014, ApJ, 794, 36
Hillenbrand, L. A., Hoffer, A. S., & Herczeg, G. J. 2013, AJ, 146, 85
Hodapp, K. W., Jensen, J. B., Irwin, E. M., et al. 2003, PASP, 115, 1388
Kochanek, C. S., Shappee, B. J., Stanek, K. Z., et al. 2017, PASP, 129, 4502
Koenig, X., Hillenbrand, L. A., Padgett, D. L., et al. 2015, AJ, 150, 100
Kostov, V. B., Powell, B. P., Rappaport, S. A., et al. 2022, ApJS, 259, 66
Kostov, V. B., Powell, B. P., Rappaport, S. A., et al. 2024, MNRAS, 527, 3995
Kounkel, M., Covey, K., Suárez, G., et al. 2018, AJ, 156, 84
Kratter, K., & Lodato, G. 2016, ARAA, 54, 271
Kuruwita, R. L., & Haugbolle, T. 2023, A&A, 674, A196
Larson, R. B. 1972, MNRAS, 156, 437
Lawson, W. A., Lyo, A.-R., & Bessell, M. S. 2009, MNRAS, 400, L29
Lee, A. T., Offner, S. S. R., Kratter, K. M., Smullen, R. A., & Li, P. S. 2019, ApJ, 887, 232
Leinert, C., Zinnecker, H., Weitzel, N., et al. 1993, A&A, 278, 129
Lightkurve Collaboration, Cardoso, J. V. de M., Hedges, C., et al. 2018, Astrophysics Source Code Library, ascl:1812.013
Lodieu, N., Dobbie, P. D., & Hambly, N. C. 2011, A&A, 527, A24
Mason, B. D., Wycoff, G. L., Hartkopf, W. I., Douglass, G. G., & Worley, C. E. 2022, Vizier Online Data Catalog: The Washington Visual Double Star Catalog
Martín, E. L., Rebolo, R., & Zapatero-Osorio, M. R. 1996, ApJ, 469, 706
Mikkola, S. 1983, MNRAS, 203, 1107
Mikkola, S. 1984a, MNRAS, 207, 115

Mikkola, S. 1984b, MNRAS, 208, 75
Offner, S. S. R., Moe, M., Kratter, K. M., et al. 2023, in ASP Conf. Ser. 534, Protostars and Planets VII, ed. S. Inutsuka et al. (San Francisco, CA: ASP), 275
Pettersson, B., Armond, T., & Reipurth, B. 2014, A&A, 570, A30
Pineda, J. E., Offner, S. S. R., Parker, R. J., et al. 2015, Natur, 518, 213
Prato, L., Ghez, A. M., Piña, R. K., et al. 2001, ApJ, 549, 590
Pratt, H., & Gledhill, J. 1880, Obs, 3, 637
Raghavan, D., McAlister, H. A., Henry, T. J., et al. 2010, ApJS, 190, 1
Reipurth, B., Clarke, C. J., Boss, A. P., et al. 2014, in Protostars and Planets VI, ed. H. Beuther et al. (Tucson, AZ: Univ. Arizona Press), 267
Reipurth, B., & Mikkola, S. 2015, AJ, 149, 145
Reipurth, B., Mikkola, S., Connelley, M., & Valtonen, M. 2010, ApJL, 725, L56
Reipurth, B., & Zinnecker, H. 1993, A&A, 278, 81
Riddle, R. L., Tokovinin, A., Mason, B. D., et al. 2015, ApJ, 799, A4
Rowden, P., Borkovits, T., Jenkins, J. M., et al. 2020, AJ, 160, 76
Sadavoy, S. I., & Stahler, S. W. 2017, MNRAS, 469, 3881
Schaefer, G. H., Hummel, C. A., Gies, D. R., et al. 2016, AJ, 152, 213
Schlawin, E., Herter, T. L., Henderson, C., et al. 2014, Proc. SPIE, 9147, 91472H
Shappee, B. J., Prieto, J. L., Grupe, D., et al. 2014, ApJ, 788, 48
Soderblom, D. R., Jones, B. F., Balachandran, S., et al. 1993, AJ, 106, 1059
Sterzik, M. F., & Durisen, R. H. 1998, A&A, 339, 95
Suárez, G., Downes, J. J., Román-Zúñiga, C., et al. 2017, AJ, 154, 14
Taylor, M. B. 2005, in ASP Conf. Ser. 347, Astronomical DataAnalysis Software and Systems XIV, ed. R. E. P. Shopbell & M. Britton (San Francisco, CA: ASP), 29
Todorov, K., Luhman, K. L., & McLeod, K. K. 2010, ApJL, 714, L84
Tody, D. 1986, Proc. SPIE, 627, 733
Tody, D. 1993, in ASP Conf. Ser. Vol. 52, Astronomical Data Analysis, Software and Systems II, ed. R. J. Hanisch et al. (San Francisco, CA: ASP), 173
Tokovinin, A. 2014, AJ, 147, A87
Tokovinin, A. 2020, AstL, 46, 612
Tokovinin, A., Mason, B. D., Mendez, R. A., & Costa, E. 2022, AJ, 164, 58
Torres, G., Ruiz-Rodriguez, D., Badenas, M., et al. 2013, ApJ, 773, A40
Torres-Robledo, S., Briceño, C., Quint, B., & Sanmartim, D. 2020, in ASP Conf. Ser. 522, Astronomical Data Analysis Software and Systems XXVII, ed. P. Ballester et al. (San Francisco, CA: ASP), 533
Vaessen, T., & van Roestel, J. 2024, A&A, 682, A164
Valtonen, M., & Karttunen, H. 2006, The Three-Body Problem (Cambridge: Cambridge Univ. Press)
van Albada, T. S. 1968a, BAN, 19, 479
van Albada, T. S. 1968b, BAN, 20, 57
Wang, J., David, T. J., Hillenbrand, L., et al. 2018, ApJ, 856, A141
Weaver, W. B., & Babcock, A. 2004, PASP, 116, 1035
White, R. J., & Basri, G. 2003, ApJ, 582, 1109
White, R. J., Ghez, A. M., Reid, I. N., & Schultz, G. 1999, ApJ, 520, 811
Whitworth, A. P. 2001, IAU Symp. 200, The Formation of Binary Stars, ed. H. Zinnecker & R. D. Mathieu (San Francisco, CA: ASP), 33
Zasche, P., Uhlař, R., Svoboda, P., et al. 2019, AJ, 158, 95
Zúniga-Fernández, S., Olofsson, J., Bayo, A., et al. 2021, A&A, 655, A15